Biomaterials Science

ROYAL SOCIETY OF CHEMISTRY

PAPER

View Article Online
View Journal | View Issue

Cite this: *Biomater. Sci.*, 2022, **10**, 549

Optimization of phospholipid chemistry for improved lipid nanoparticle (LNP) delivery of messenger RNA (mRNA)†

Ester Álvarez-Benedicto, Lukas Farbiak, Martha Márquez Ramírez, Xu Wang, Lindsay T. Johnson, Osamah Mian, Erick D. Guerrero and Daniel J. Siegwart *

Lipid nanoparticles (LNPs) have been established as an essential platform for nucleic acid delivery. Efforts have led to the development of vaccines that protect against SARS-CoV-2 infection using LNPs to deliver messenger RNA (mRNA) coding for the viral spike protein. Out of the four essential components that comprise LNPs, phospholipids represent an underappreciated opportunity for fundamental and translational study. We investigated this avenue by systematically modulating the identity of the phospholipid in LNPs with the goal of identifying specific moieties that directly enhance or hinder delivery efficacy. Results indicate that phospholipid chemistry can enhance mRNA delivery by increasing membrane fusion and enhancing endosomal escape. Phospholipids containing phosphoethanolamine (PE) head groups likely increase endosomal escape due to their fusogenic properties. Additionally, it was found that zwitterionic phospholipids mainly aided liver delivery, whereas negatively charged phospholipids changed the tropism of the LNPs from liver to spleen. These results demonstrate that the choice of phospholipid plays a role intracellularly by enhancing endosomal escape, while also driving organ tropism *in vivo*. These findings were then applied to Selective Organ Targeting (SORT) LNPs to manipulate and control spleen-specific delivery. Overall, selection of the phospholipid in LNPs provides an important handle to design and optimize LNPs for improved mRNA delivery and more effective therapeutics.

Received 16th September 2021,
Accepted 22nd November 2021

DOI: 10.1039/d1bm01454d

rsc.li/biomaterials-science

Introduction

Lipid nanoparticles (LNPs) are an established concept for nucleic acid delivery.[1–9] The first siRNA therapeutic approved by the U.S. FDA in 2018, called Onpattro, was a LNP formulation that delivers siRNA into liver hepatocytes.[10] More recently, LNP delivery of mRNA has gained timely importance, including utility in multiple COVID-19 vaccines against SARS-CoV-2.[11] LNPs are typically composed of four key components: ionizable cationic lipids, zwitterionic phospholipids (PL), cholesterol, and poly(ethylene glycol) (PEG) lipids (Fig. 1A). Fundamentally, the ionizable cationic lipid plays an important role since it can be positively charged below its pK_a to mediate loading of negatively charged RNA during self-assembly into LNPs, uncharged at neutral pH to minimize toxicity, and become positively charged again following cellular uptake to facilitate endosomal escape as the endosomal pH decreases.[12,13] Because of its active role in nucleic acid delivery, ionizable lipids have been the primary focus of LNP study and development.[4,7,14–20]

Recently, however, it has become clearer that all four components of LNPs play essential roles at various stages of the delivery process. For example, variants of cholesterol[21,22] and PEG lipids[23–28] have been shown to modulate LNP physical properties, nanostructure, and ultimate efficacy. Zwitterionic phospholipids are commonly referred to as "helper lipids", implying that they are less critical for efficacy. While PLs have been used and studied in small molecule drug and siRNA containing liposomes for decades,[29–32] there is more to learn in understanding their location and function within mRNA containing LNPs and in cells. Both Onpattro and the mRNA vaccines use 1,2-distearoyl-*sn-glycero*-3-phosphocholine (DSPC) as the "helper lipid" in their LNP formulation following its traditional use in liposome-mediated drug delivery.[33–41] Computational and experimental studies have suggested that phospholipids may aid in the solubilization of RNAs inside of aqueous pockets within LNPs.[42,43] We, and others, have further studied how the solubilizing forces may improve LNP

Department of Biochemistry, Simmons Comprehensive Cancer Center, The University of Texas Southwestern Medical Center, Dallas, Texas 75390, USA.
E-mail: Daniel.Siegwart@UTSouthwestern.edu

†Electronic supplementary information (ESI) available: Supporting Fig. S1–S11 and additional references. See DOI: 10.1039/d1bm01454d

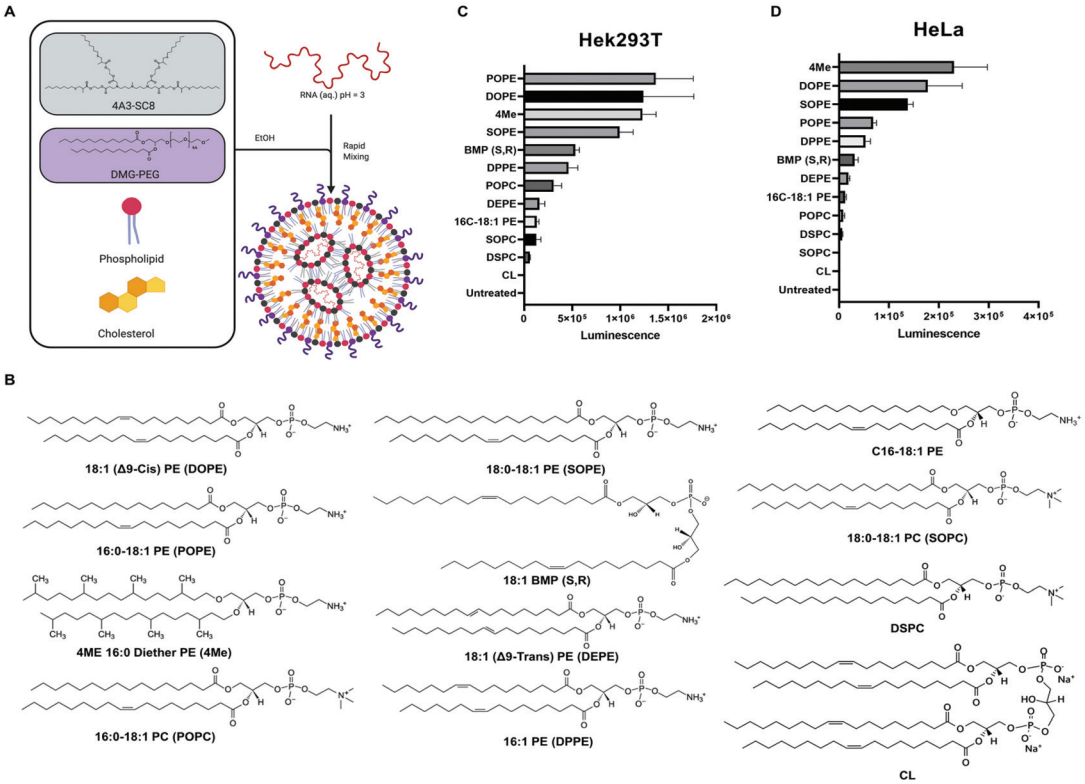

Fig. 1 Phospholipids with PE headgroup increase LNP-mediated mRNA delivery. (A) Model illustrating LNP components and formulation process. (B) Structure of phospholipids used for *in vitro* mRNA delivery screen. Results for luciferase protein activity following delivery of firefly luciferase mRNA to HEK293T cells (C) and HeLa cells (D).

construction.[43–45] We showed, for example, that increasing molar proportions of phospholipid into LNPs improved delivery efficacy of sgRNA and mRNA, but did not affect siRNA delivery efficacy (see ESI in ref. 43). Zwitterionic PLs are thought to have an assistive role during LNP assembly by stabilizing electrostatic interactions between ionizable cationic lipids, RNA, and water molecules.[25,46] However, less is known about their potential biological or physical intracellular behaviour. Thus, more work remains to be done to better understand the impact of phospholipids on LNP delivery of mRNAs.

Natural and naturally-derived PLs have been used for decades in liposomes for various drug delivery applications with typically high biocompatibilities.[47] It remains intriguing to consider how cells use a variety of natural lipids in various cellular membranes, suggesting a broad space for lipid discovery and application to LNPs. Eukaryotic membranes are rich in glycerophospholipids such as phosphatidylcholine (PC), phosphatidylethanolamine (PE), and phosphatidylserine (PS).[48] Depending on the location within cells, the PL composition varies significantly. The plasma membrane is rich in sphingolipids and sterols, whereas endosomal membranes are rich in bis(monoacylglycerol)phosphate (BMP).[48] Lipids with PC and PS groups provide bilayer membrane stability, whereas PE-lipids introduce membrane curvatures and increase tension, which in turn facilitates membrane fusion.[30,49,50] These observations concerning the compositions of natural membranes within cells, coupled to the essential endosomal escape requirement facilitated by LNPs, prompted us to consider how inclusion of alternative phospholipids in LNPs might serve as active lipids to improve cellular delivery of mRNAs.

RNA therapies used in the clinic, such as Onpattro and the first-in-class SARS-CoV-2 vaccines, use DSPC as the PL in their four-component LNP formulation.[10,11] Despite DSPC's wide utility and proven efficacy in LNP formulations for siRNA delivery and COVID-19 vaccines, substituting DSPC with 1,2-dioleoyl-*sn-glycero*-3-phosphoethanolamine (DOPE) greatly increased luciferase mRNA delivery *in vivo* up to four-fold.[44,51,52] Thus, phospholipid identity can significantly affect mRNA delivery suggesting PLs play a functional role in nucleic acid delivery. Phospholipids with PC headgroups can adopt a cylinder phase that forms stable lipid bilayer.[47] In contrast, a lipid with PE headgroups can adopt a cone shape that transitions to hexagonal conformation (H_{II}) associated with membrane fusion properties.[47] An enhanced fusion of polyplexes with the plasma membrane which resulted in greater transfection efficiency was observed when substituting DSPC for DOPE.[53] Based on these precedents, one can hypothesize that the differences in phospholipid structure may increase RNA delivery potency by physical and/or biological mechanisms.

To study the role of phospholipids in LNPs, we decided to screen several structurally diverse phospholipids with PE and PC headgroups, varying chain length, degree of saturation,

and methyl substitution (Fig. 1B). Additionally, we included lipids that are unique to organelle membranes, such as BMP and cardiolipin (CL), exclusive to endosome and mitochondrial membranes, respectively. Both lipids have unique chemical structures that could provide benefits for endosomal escape due to similarities with the endosomal membrane or disrupt the integrity of the endosomal membrane due to striking structural differences. Additionally, BMP and CL have molecular shapes of inverted cone and cone, respectively, which produce similar effects to PE lipids.[47]

Overall, the results described here demonstrate that phospholipids have a functional role in nucleic acid delivery. Phospholipids with PE head groups were consistently more efficient for *in vitro* and *in vivo* mRNA delivery. Moreover, DOPE-containing LNPs enabled significantly more endosomal escape compared to DSPC-containing LNPs, which appeared to be more sequestered in lysosomes after endocytosis. Additionally, LNPs with negatively charged phospholipids had an increased spleen targeting effect *in vivo* compared to neutral phospholipids that were most effective in liver delivery of luciferase mRNA. Therefore, we conclude that all components of the LNP play an essential role and should be systematically studied for mRNA delivery. Further knowledge on the role PLs play on LNP-mediated nucleic acid delivery could lead to improved delivery of mRNA therapeutics including current SARS-CoV-2 and future vaccines,[54] as well as to set the foundation for the development of novel vaccines and therapeutics against a variety of diseases.[55]

Materials and methods

Materials

Lipids for LNPs. 1,2-Distearoyl-*sn-glycero*-3-phosphocholine (DSPC), 1,2-dioleoyl-*sn-glycero*-3-phosphoethanolamine (DOPE), 1-palmitoyl-2-oleoyl-*sn-glycero*-3-phosphoethanolamine (POPE), 1,2-di-*O*-phytanyl-*sn-glycero*-3-phosphoethanolamine (4ME), 1-palmitoyl-2-oleoyl-*glycero*-3-phosphocholine (POPC), 1-stearoyl-2-oleoyl-*sn-glycero*-3-phosphoethanolamine (SOPE), 1,2-dielaidoyl-*sn-glycero*-3-phosphoethanolamine (DEPE), 1-hexadecyl-2-(9*Z*-octadecenoyl)-*sn-glycero*-3-phosphoethanolamine (C16–18 : 1), 1-stearoyl-2-oleoyl-*sn-glycero*-3-phosphocholine (SOPC), *N*-(7-nitrobenz-2-oxa-1,3-diazol-4-yl)-phosphatidylethanolamine (NBD-PE), *N*-(lisamine Rhodamine B sulfonyl)-phosphatidylethanolamine (Rh-PE), cholesterol (Chol), sphingomyelin (SM) from porcine brain, phosphatidylinositol (PI) from soybean, 1,2-dioleoyl-*sn-glycero*-3-phosphocholine (PC), sn-(3-(9*Z*-octadecenoyl)-2-hydroxy)-glycerol-1-phospho-*sn*-3′-(1′-(9*Z*-octadecenoyl)-2′-hydroxy)-glycerol (BMP-S, R), and *sn*-(3-oleoyl-2-hydroxy)-glycerol-1-phospho-*sn*-1′-(3′-oleoyl-2′-hydroxy)-glycerol (BMP-S,S) were purchased from Avanti Polar Lipids (Alabaster, AL). Cholesterol was purchased from Sigma Aldrich. DMG-PEG2000 (Sunbright GM-020) was purchased from NOF America Corporation. The dendrimer ionizable amino lipid 4A3-SC8 was synthesized in our lab according to a previously reported protocol.[17]

Reagents for biological assays. CleanCap Fluc mRNA, CleanCap mCherry mRNA, and CleanCap Cyanine 5 Fluc mRNA were purchased from TriLink Biotechnologies. QUANT-iT Ribogreen reagent, LysoTracker Green, and Hoechst 33342 were purchased from ThermoFisher Scientific. One-Glo + Tox were purchased from Promega. HEK293T cells and HeLa cells were purchased from ATCC.

Cell culture. Dulbecco's Modified Eagle Medium (DMEM) containing high glucose, sodium pyruvate, L-glutamine, and phenol red was purchased from ThermoFisher Scientific. Trypsin-EDTA (0.25%) and fetal bovine serum (FBS) (10%) were purchased from Sigma-Aldrich. Penicillin–streptomycin was purchased from Fisher Scientific.

Animal studies. All experiments were approved by the Institutional Animal Care & Use Committee (IACUC) of The University of Texas Southwestern Medical Center and were consistent with local, state, and federal regulations as applicable.

Methods

Formulation of 4A3-SC8 four-component LNPs. 4A3-SC8 LNPs were prepared by rapid hand mixing of acidic aqueous solution and ethanol solution. The ethanol solution contained 4A3-SC8, cholesterol, variable phospholipids, and DMG-PEG2000 in a molar ratio of 38.5 : 30 : 30 : 1.5. The mRNA was dissolved in the 100 mM citrate buffer pH 3.0. The aqueous solution and ethanol solution were rapidly mixed for 30 seconds at a 3 : 1 volume ratio and were incubated at room temperature for 15 min to allow LNP assembly. For *in vitro* experiments, PBS solution was added to reach a 10 mM citrate concentration. For *in vivo* experiments, LNPs were purified by dialysis in sterile PBS with 3.5 kDa cut-off for 2 hours. The mol ratio of 4A3-SC8 to mRNA was 10 000 : 1 and the weight ratio was 23 : 1.

Formulation of 4A3-SC8 five-component SORT LNPs. 4A3-SC8 SORT LNPs were prepared by rapid hand mixing of acidic aqueous solution and ethanol solution. The ethanol solution contained 4A3-SC8, DOPE, cholesterol, DMG-PEG, and variable phospholipids in a molar ratio of 15 : 15 : 30 : 30 : 3 : x, where x was varied to change the molar percentage of the SORT phospholipid from 5% to 40% (x = 3.315, 7, 15.75, 27, 42). SORT LNPs were purified by dialysis in sterile PBS with 3.5 kDa cut-off for 2 hours. The mol ratio of 4A3-SC8 to mRNA was 10 000 : 1 and the weight ratio was 23 : 1.

C12-200 LNP formulation. C12-200 LNPs were prepared by rapid hand mixing of aqueous solution and ethanol solution. The ethanol solution contained C12-00, cholesterol, DMG-PEG, and variable phospholipids in a molar ratio of 50 : 38.5 : 1.35 : 10. The mol ratio of C12-200 to mRNA used was 10 000 : 1 which is equivalent to a weight ratio of 25 : 1.

Characterization of LNPs. Size and zeta potential of LNPs were measured using a Malvern Zetasizer. Size and polydispersity index were measured by dynamic light scattering (He–Ne laser, λ = 632 nm; detection angle = 173°) using 100 μL of fresh LNP dispersion. Zeta potential was measured after diluting LNPs to 800 μL with 1× PBS. RNA encapsulation was measured using QUANT-iT Ribogreen assay (ThermoFisher Scientific) fol-

lowing the established protocol. Briefly, an RNA standard curve solution was prepared in PBS with concentrations from 0–10 ng μL^{-1}. In a black bottom 96-well plate, 5 μL of standard solution or LNP were added per well (n = 4). To measure free/unbound RNA, 50 μL of 1× Ribogreen solution were added to each well. The solutions were incubated for 5 min under constant shaking at 120 rpm and the fluorescent signal was measured in a plate reader (Tecan). To measure total RNA, 50 μL of 0.5% Triton X-100 was added per well. The plate was incubated under constant shaking for 5 min and fluorescence was measured. The percentage of encapsulated RNA was calculated as 100 × (ng of total RNA − ng of free RNA)/ng of total RNA.

Gel retardation assay. 4A3-SC8 LNPs were formulated as stated above using Cy5-labeled mRNA. Samples were loaded into a 1.5% agarose gel alongside free Cy5-mRNA. A BioRad PowerPac Basic was used to run the gel at 60 V for 60 min. An IVIS Lumina system (PerkinElmer) was used to image the gel.

4A3-SC8 LNP stability studies. After LNPs were formulated, stability was measured by determining size and polydispersity index using dynamic light scattering (He–Ne laser, λ = 632 nm; detection angle = 173°) every 24 hours for a total of 72 hours, both at room temperature and 4 °C.

Transmission electron microscopy (TEM). 4A3-SC8 LNPs were prepared by hand mixing using the phospholipids and the same molar ratios stated previously. LNPs were the dialysed in 2 L of MilliQ Water to remove ethanol and salts present in the solution. Volumes after dialysis were adjusted so the concentration of total lipid was 1 mg mL^{-1}. Samples were loaded into 200-mesh copper carbon grids (PELCON no. 160) and imaged using FEI Tecnai G2 Spirit Biotwin TEM.

***In vitro* luciferase expression and cell viability.** HEK293T and HeLa cells were seeded at 1 × 10^4 and 5 × 10^3 cells per well, respectively (100 μL final volume, DMEM 10% FBS) in a white bottom 96-well plate. After 24 h, cells were transfected with LNPs (12.5 ng of Fluc mRNA) and 100 μL of fresh DMEM medium (10% FBS) were added. Cells were incubated 48 h and ONE-Glo + Tox (Promega) were used to measure luciferase expression and cell viability using Promega's standard protocol.

Transfection efficiency and cellular uptake. HeLa and HEK293T cells were treated with mCherry mRNA to quantify the percentage of transfection by flow cytometry. Cells were seeded at 1.75 × 10^5 cells per well in a 6-well plate (1 mL final volume, DMEM 10% FBS). After 24 h, cells were treated with LNPs (250 ng mCherry mRNA) and 1 mL of fresh DMEM (10% FBS was added). Cells were washed with PBS, trypsinized for 3 min at 37 °C, neutralized with 1 mL of DMEM, centrifuged at 300g for 5 min, washed with cold PBS twice, and diluted in 500 μL of cold PBS. Finally, cells were kept on ice until they were analyzed by a LSRFortessa flow cytometer (BD Biosciences). Uptake of LNPs was measured after treatment with Cy5-labeled Fluc mRNA (250 ng) LNPs. The same protocol described above was used to measure percentage of cellular uptake.

Colocalization of LNPs with endosomes. Confocal imaging was performed to study endosomal escape of DOPE- and DSPC-LNPs. HeLa cells were seeded into Lab-Tek Chambered cover glass at a density of 1 × 10^4 cell per chamber (final volume 400 μL DMEM 10% FBS). After 24 h, medium was removed, 60 μL of Cy-5 labelled LNP (280 ng) were added and 340 μL of fresh media was added. Cells were washed three times with PBS, and stained with Lysotracker Green (1 : 3000 dilution) and Hoechst 33342 (0.1 mg ml^{-1}) for 15 min at 37 °C. Finally, cells were imaged by confocal microscopy (LSM 700, Zeiss). Pearson's coefficient was calculated using PSC Colocalization plugin for Image J following the protocol previously described.[56]

Lipid fusion FRET assay. Lipid fusion with endosome and plasma membrane mimicking liposomes was determined by a FRET assay. Briefly, DOPE-conjugated FRET probes, NBD-PE and N-Rh-PE (Avanti Polar Lipids), were formulated into the same mimicking liposome reducing NBD fluorescence due to FRET to N-Rh-PE. Plasma membrane mimicking liposomes were prepared by mixing of DOPC, DOPE, NBD-PE, N-Rh-PE, Sphingomyelin (SM), and cholesterol (molar ratio 20 : 18 : 1 : 1 : 20 : 30) in chloroform followed by 3 h of dry vacuum to give a thin layer. The thin layer was resuspended in PBS buffer pH 7.4 for a 1 mM final concentration of total lipid and sonicated for 20 min (10 s sonication, 20 s rest). Endosome mimicking liposomes were prepared mixing BMP, DOPC, DOPE, NBD-PE, N-Rh-PE, PI (molar ratio 10 : 50 : 18 : 1 : 1 : 10) in chloroform. Liposomes were prepared following the same procedure described before. LNPs were prepared as described previously. In a black bottom 96-well plate, 100 μL of PBS were added per well with pH 7.4 or pH 5.5 for plasma membrane and endosome mimicking liposomes, respectively. Then, 1 μL of 1 mM mimicking liposomes was added to each well and LNP with different formulations (n = 3, per formulation) were added for a ratio of 1 : 10 (liposome : LNP by concentration). The control for minimal fluorescence (F_{min}) was wells untreated with LNP; and the control for maximum fluorescence (F_{max}) was treated with 8 μL of Triton X-100. Plate was incubated at 37 °C for 5, 15, 30, 45, 60, and 90 min. Finally, fluorescence for each time point was measured in a plate reader (Tecan), $\lambda_{excitation}$ = 465 nm, and $\lambda_{emission}$ = 520 nm. Lipid fusion was calculated as $(F_{sample} - F_{min})/(F_{max} - F_{min}) \times 100$.

***In vivo* luciferase mRNA delivery.** All experiments were approved by the Institution Animal Care and Use Committees of The University of Texas Southwestern Medical Center and were consistent with local, state, and federal regulations as applicable. Normal wild-type C57BL/6 female mice were maintained as a colony. When mice reached a body weight between 18–20 g, LNPs formulated with Fluc mRNA were injected IV at a dose of 0.03 mg kg^{-1}. After 6 h, D-luciferin was injected (150 mg kg^{-1}) IP. After 5 min, organs (lungs, liver, kidneys, and spleen) were dissected, and luciferase luminescence was imaged using an IVIS Lumina system (PerkinElmer). Luminescence was quantified as total luminescence (p s^{-1}) and average luminescence of total organ areas (p s^{-1} cm^{-2} sr^{-1}).

Results and discussion

Selection of PLs and LNP formulation

Our lab and others have studied how the composition of LNPs should be engineered to productively deliver diverse nucleic acids including siRNA,[17] miRNA,[17] mRNA,[52,57,58] sgRNA,[43,59] and ribonucleoproteins.[60] The LNPs used here are composed of four core components: dendrimer-based ionizable amino lipids, cholesterol, zwitterionic phospholipids, and PEG lipids. Dendrimer-based ionizable amino lipids have been systematically tested to determine the structure–activity relationship (SAR) between the amine core (4A3), the alkyl peripheries (SC8), and the nucleic acid delivery potential. 4A3-SC8 has been consistently active for the delivery of short (siRNA)[17] to long (mRNA, sgRNA, ssDNA) nucleic acids.[61,62]

A systematic series of LNPs were prepared by introducing a variable phospholipid in each formulation while maintaining the ionizable cationic lipid (4A3-SC8), cholesterol, and PEG-lipid (PEG-DMG) constant. In all LNPs, the molar ratio of the components was fixed at 4A3-SC8/cholesterol/PEG-DMG/variable phospholipid = 38.5/30/1.5/30 (mol mol^{-1}). This strategy allowed us to systematically test the mRNA delivery efficiency of each phospholipid as a single variable in the context of LNPs. Each formulated LNP was characterized with respect to diameter, polydispersity index (PDI), zeta potential, and mRNA encapsulation (Fig. S1†). All formulated LNPs had RNA encapsulation above 80%, with the exception of CL-LNP which exhibited 50% encapsulation efficiency (Fig. S1A†). Zeta potential values for all LNPs were between −2 mV and −4 mV, (Fig. S1B†). LNPs were similar in size, approximately 100 nm (Fig. S1C†), and PDI values were below 0.2, indicating uniform size across all LNPs (Fig. S1D†). LNPs were stable at room temperature and at 4 °C for at least 72 hours regardless of the phospholipid used in the formulation (Fig. S2†). We concluded that the identity of the phospholipids studied in this manuscript did not significantly affect LNP stability. A gel retardation assay examining the LNPs and free mRNA shows that all LNPs successfully encapsulated mRNA and inhibited mRNA migration compared to free mRNA (Fig. S3†). The results agree with results determined by the Ribogreen assay (Fig. S1A†). Lastly, we used Transmission Electron Microscopy (TEM) to image the various LNPs as a function of the incorporated phospholipid (Fig. S4†). These results showed that there are no appreciable differences in morphology observed when different phospholipids are used to formulate the LNPs. All LNPs were spherical in shape. No obvious trends were

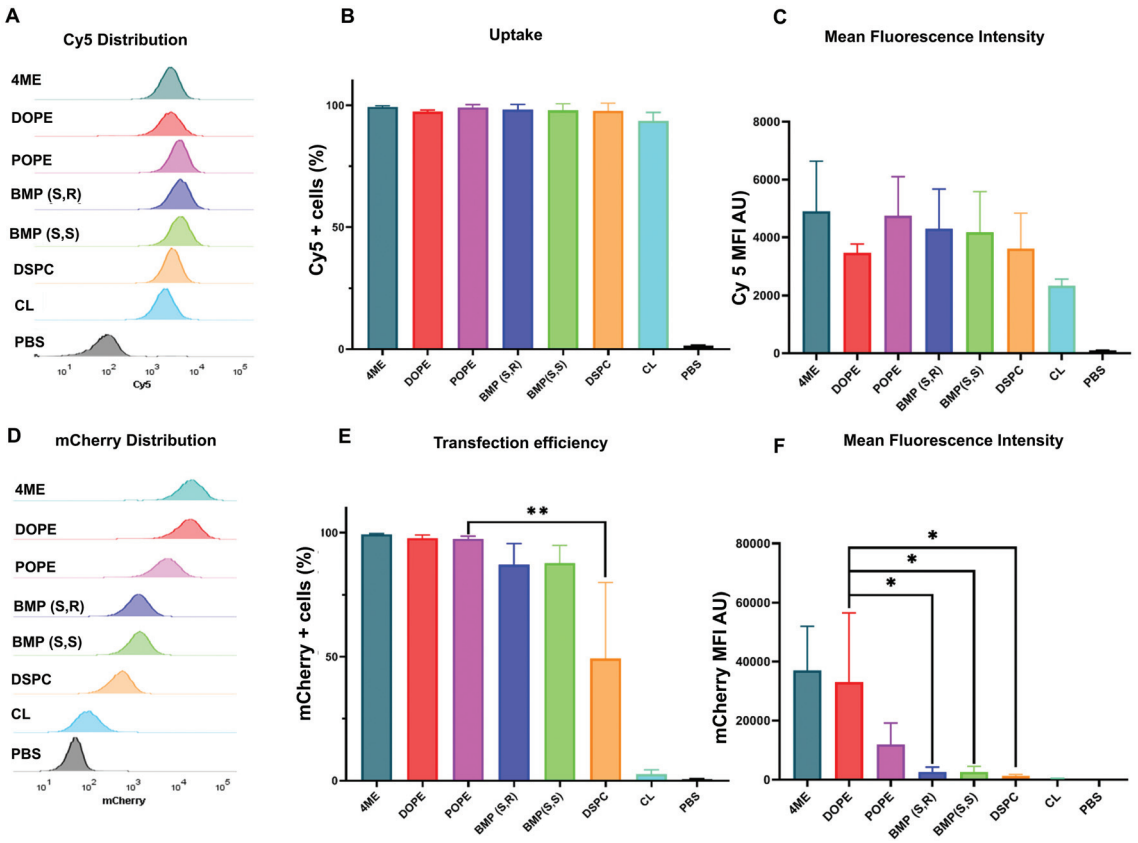

Fig. 2 Uptake of Cy5-LNPs is not affected by phospholipid identity. Flow cytometry was used to determine (A) distribution of Cy5 fluorescence, (B) percentage of Cy5 positive cells, and (C) mean fluorescence intensity. Distribution of mCherry fluorescence (D), percentage of mCherry positive cells, (E) and mean fluorescence intensity of each LNP (F) obtained by flow cytometry after 48 h incubation of HeLa cells with Cy5-labeled mRNA-LNP (250 ng $N = 4 \pm$ stdev, one-way ANOVA **** $p < 0.0001$, Tukey's test ** $p < 0.001$, * $p < 0.01$.

observed in the physical characterization that explained the differences observed in the *in vitro* mRNA delivery (Fig. 1).

SAR determination of zwitterionic PLs for *in vitro* mRNA delivery

We initially evaluated each LNP for its ability to deliver luciferase (Luc) mRNA to two representative cell lines as a first readout. Waterfall plots revealed that PE-containing lipids (DOPE, POPE, SOPE, 4ME) were more efficient at *in vitro* mRNA delivery in HEK293T and HeLa cell lines than PC-containing lipids (Fig. 1C and D, respectively). Acknowledging that *in vitro* delivery potential does not always translate to *in vivo* delivery potential,[28] top-performing phospholipids in LNPs contained hydrophobic chains with unsaturated bonds. Whether one chain or both chains contained an unsaturation seemed to have no difference in mRNA delivery efficiency. Additionally, the bulkier methyl-substituted chains present in 4ME facilitated mRNA delivery to the same degree of unsaturated/saturated chains. BMP (S, R) enhanced delivery compared with standardly used DSPC but less so when compared to top PE-containing lipids. The fusogenic nature of PE lipids may enhance *in vitro* LNP delivery of mRNA. LNPs can be formulated with different ionizable amino lipids, such as the benchmark C12-200, that might affect how PLs impact mRNA delivery. We found that C12-200 LNPs formulated with DOPE outperformed DSPC formulated C12-200 LNPs (Fig. S5†). These results suggest phospholipids could enhance LNP uptake resulting in enhanced delivery of mRNA into the cytosol. Alternatively, it could be a result of enhanced LNP fusion with endosomal membranes causing their destabilization and increasing endosomal escape of mRNA. To further investigate these questions, we quantified cellular uptake and endosomal escape.

Uptake and transfection of LNPs for *in vitro* mRNA delivery

After identification of the top- and worst-performing LNPs, we set out to determine whether the limiting step for effective delivery could be uptake of LNPs or endosomal escape. LNPs enter cells through endocytosis pathways. For effective transfection, mRNA must escape the endosomes before they fuse with lysosomes and the mRNA is degraded. To quantify uptake, LNPs were formulated with Cy5-labeled mRNA to measure the percentage of cells that were positive for Cy5 fluorescence. Mean fluorescence intensity (MFI) was used to measure the amount of LNPs that were endocytosed by the cells. These results were coupled to parallel experiments involving delivery of mCherry mRNA. mCherry positive cells allowed us to quantify the effective transfection of mRNA, which reflects the amount of mRNA that escaped the endosome and was translated into protein. The distribution of Cy5 fluorescence showed there was no difference between the uptake of LNPs formulated with different phospholipids (Fig. 2A). This was confirmed by the number of Cy5 positive cells (Fig. 2B) and the Cy5 MFI observed for each treatment group (Fig. 2C). With respect to functional delivery, mCherry fluorescence emission matched the results of the *in vitro* luminescence screen (Fig. 2D–F). The same experiments were performed using HEK293T cells (Fig. S6†) confirmed the results observed in HeLa cells. Overall, we found that LNP

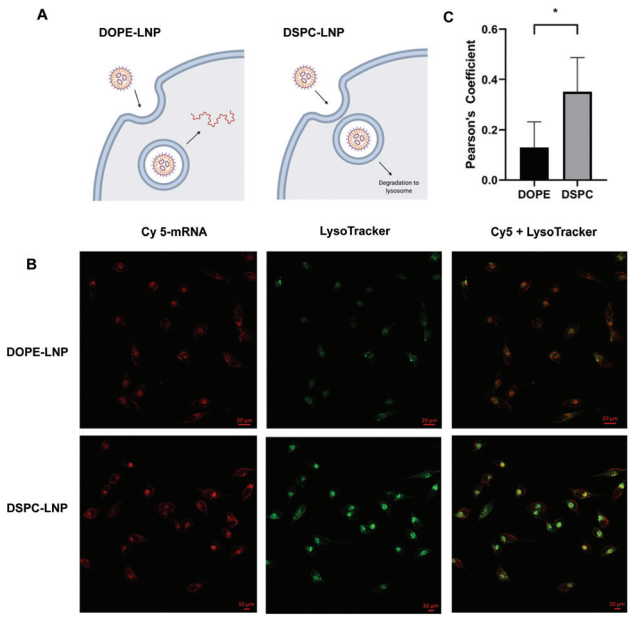

Fig. 3 DOPE enhances endosomal escape. (A) Proposed model of endosomal escape for DOPE-LNP and DSPC-LNP. (B) Representative images of HeLa cells treated with Cy5-labeled mRNA (280 ng) LNPs (red), stained with LysoTracker (green) imaged 24 h later using confocal microscopy. (C) Pearson coefficient of colocalization between LNPs (red) and lysosomes (green) obtained using the PSC Colocalization plugin from ImageJ. (C) $N = 4 \pm$ stdev, Unpaired t test * $p < 0.05$.

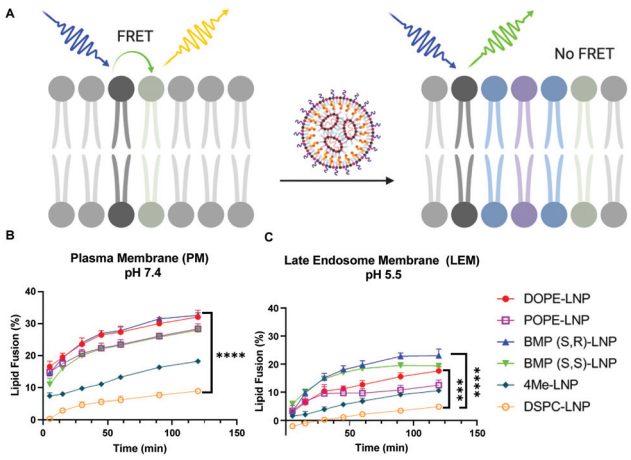

Fig. 4 DOPE- and BMP-LNP enhance lipid fusion with liposome-mimicking biological membranes. (A) Lipid fusion model of biological membrane mimic in which a liposome containing a quencher lipid (black) and fluorescent lipid (light green) is mixed with unlabeled LNP (blue). Separation of the FRET pair increases 520 nm emission measured in a plate reader. Results of lipid fusion experiments at different time points after incubation of LNPs with plasma membrane (B) and endosomal membrane (C) mimicking liposomes. $N = 3 \pm$ stdev, one-way ANOVA **** $p < 0.0001$, Tukey's test ** $p < 0.001$, * $p < 0.01$.

uptake was not dependent on PL identity and did not explain the differences observed in effective mCherry mRNA delivery. These results suggest that phospholipids may play a role in facilitating the endosomal escape of mRNA. We therefore hypothesized that the increased endosomal escape was due to enhanced fusion with the endosomal membrane.

Endosomal escape of DOPE- and DSPC-LNPs

Flow cytometry experiments of Cy5-labeled LNPs ruled out uptake as the limiting step for increased mRNA delivery observed with the different formulations. This led us to consider that PLs may enhance endosomal escape of mRNA. If endosomal escape is enhanced by PLs, colocalization of Cy5-labeled LNPs and lysosomes would likely be affected (Fig. 3A). Confocal microscopy was used to quantify the colocalization between lysosomes and DOPE- and DSPC-LNPs, the top- and worst-performing LNPs, respectively. Fig. 3B includes representative confocal images of cells labelled with LysoTracker green and treated with Cy5 labelled DSPC- or DOPE-LNPs. The Pearson correlation coefficient was used to measure the colocalization of lysosomes and LNPs. The Pearson coefficient can have values from −1 to 1, values close to −1 indicate the two signals oppose themselves; 0, no colocalization; and 1, perfect colocalization.[63] Larger sized images and additional images used to calculate the Pearson's Coefficient are included in Fig. S7 and S8.† The Pearson's coefficient values are listed in Fig. S9.† DSPC-LNPs had a higher coefficient than DOPE-LNPs (Fig. 3C), indicating that DSPC-LNPs remain more trapped in the lysosomes failing to deliver mRNA into the cytosol adequately.

LNP fusion with membrane mimicking liposomes

Uptake and transfection experiments led us to hypothesize that PLs in LNPs could be enhancing endosomal escape. This was confirmed by higher colocalization of DSPC-LNPs with lysosomes, which have consistently achieved the lowest levels of mRNA transfection. In contrast, DOPE-LNPs had lower colocalization with lysosomes. PE lipids have been highlighted for their ability to change their conformation from cone shape to H_{II} at endosomal pH, which creates membrane instability and promotes fusion.[50] We set out to determine if the fusogenic nature some PLs would enhance LNP mixing with membrane mimicking liposomes. This would allow us to further understand PL interactions with biological membranes in the context of LNPs and determine whether phospholipids can enhance endosomal escape in an *in vitro* model system.

The lipid content (molar percentage) of the plasma membrane (PM) and the late endosome membrane (LEM) were mimicked, such that model plasma membrane liposomes had

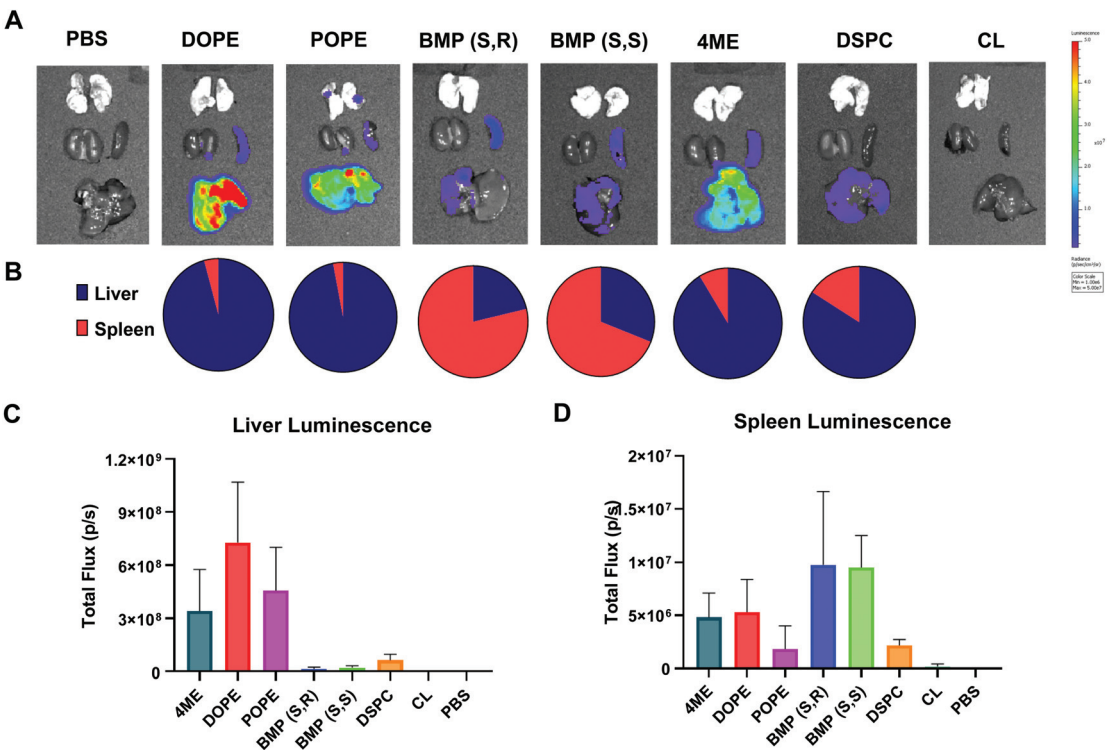

Fig. 5 DOPE-, POPE-, and 4ME-LNPs are liver predominant whereas BMP-LNPs are spleen predominant. Female C57BL/6 were injected 0.03 mg kg^{-1} Fluc mRNA IV and imaged 6 h later after IP injection of luciferin. (A) IVIS Lumina imaging of dissected organs after IV injection of Fluc mRNA (0.03 mg kg^{-1}). (B) Liver to spleen ratio of luminescence. Quantification of total and average luminescence in liver (C) and spleen (D). $N = 3 \pm$ stdev, one-way ANOVA **** $p < 0.0001$, Tukey's test ** $p < 0.001$, * $p < 0.01$.

a higher concentration of cholesterol and phosphatidylserine, whereas late endosome model membranes were rich in BMP.[64] Analogs of DOPE N-Rh-PE and NBD-PE—fluorophore and quencher, respectively—were included to label the resulting liposomes and enable membrane fusion detection *via* FRET. The dequenching of N-Rh-PE measured lipid fusion as a result of LNP-induced mixing with liposomes (Fig. 4A).

PE-containing LNPs, as well as BMP-LNPs, had higher lipid mixing with both PM (Fig. 4B) and LEM (Fig. 4C) liposome model membranes. DSPC-LNPs consistently displayed the weakest ability to fuse with membranes. These results agree with previous reports that highlight DOPE's fusogenic nature.[47,53] In contrast, DSPC has a molecular shape that resembles a cylinder that provides stability to bilayer membranes.[30] The Pearson's coefficient values obtained in Fig. 3B indicate that DSPC-LNPs colocalize with lysosomes more than DOPE-LNP. The lipid mixing results—taken together with the lysosomal colocalization coefficients—further suggest that PE-formulated LNPs enhance endosomal escape. Conversely, due to DSPC-LNP's lack of lipid mixing, these LNPs are less able to escape the endosomes and less mRNA is delivered effectively to the cytosol.

Optimized LNPs delivered mRNA *in vivo*

After characterizing LNP-mediated mRNA delivery efficacy *in vitro*, we next studied whether the results obtained translated *in vivo*. Organ luminescence was quantified 6 hours after IV injection of low dose 0.03 mg kg^{-1} Luc mRNA in LNPs with variable PLs. The 6-hour time point was used for all *in vivo* experiments because it has been previously determined to be the time point with highest protein expression after mRNA delivery.[52] DOPE-, POPE-, and 4ME-LNPs achieved the highest luminescence overall, which targeted mainly the liver (Fig. 5A and C). BMP-LNPs did not have luminescence as high as PE-containing LNPs (Fig. 5A and C). Interestingly, BMP-LNPs predominantly delivered to the spleen (Fig. 5B). Overall, PE-containing LNPs outperformed BMP- and PC-containing LNPs both *in vitro* and *in vivo*. BMP-based LNPs could provide an advantage for immune cell delivery as they also outperformed PC-LNPs and offered spleen tropism.

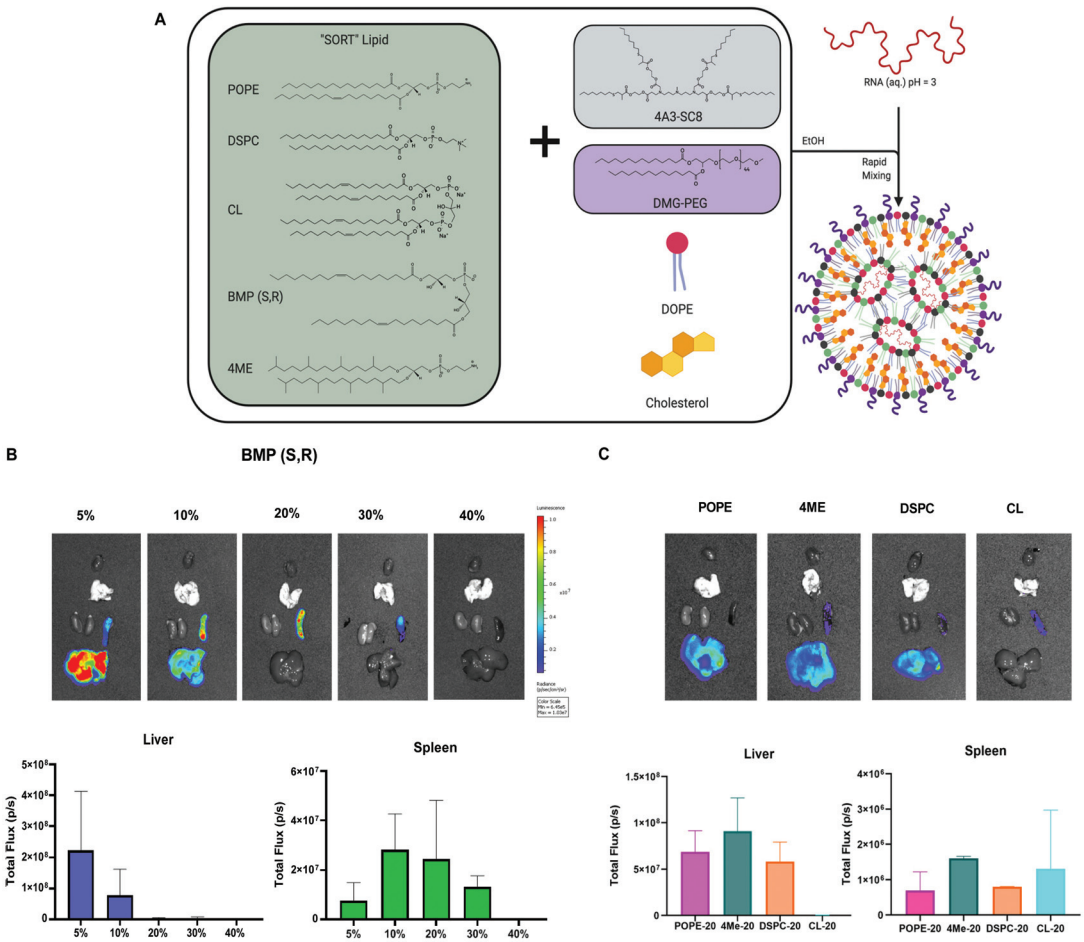

Fig. 6 Phospholipids function in SORT LNPs to drive spleen and liver organ targeting. (A) Model of SORT LNP composition and formulation process. (B) Evaluation of anionic BMP phospholipid as a SORT molecule for spleen and liver mRNA delivery. (C) Evaluation of zwitterionic phospholipids as SORT molecules.

Application of PLs to the formation of selective ORgan targeting (SORT) LNPs

Our lab recently developed a strategy called Selective ORgan Targeting (SORT), wherein the addition of a SORT molecule to LNPs creates SORT LNPs that can target specific organs including the liver, lungs, and spleen (Fig. 6A).[57–60] We discovered that incorporation of a SORT lipid (*e.g.* permanently cationic lipids, anionic lipids, zwitterionic lipids, and ionizable amino lipids) enables tissue-specific gene delivery and gene editing as a function of the chemistry and amount of the added supplemental molecule. Notably, inclusion of anionic lipids promoted exclusive protein expression in the spleen. From our results in Fig. 5A and B, the four-component formulation that contained anionic BMP exhibited preference for spleen delivery over liver delivery and could be considered a SORT LNP. BMPs are negatively charged lipids and aid spleen delivery, which is consistent with our previous results.[59] Therefore, we decided to further explore the role of BMP as a SORT molecule in five-component LNPs to increase efficacy.

We formulated LNPs using 4A3-SC8 : DOPE : cholesterol : PEG following the molar ratios of the basic SORT LNP, 15 : 15 : 30 : 3. Next, we titrated in BMP to achieve 5, 10, 20, 30 and 40% of the total lipid composition. A table summarizing the molar ratios is present in Fig. S10.† Each SORT LNP was characterized with respect to diameter, polydispersity index (PDI), zeta potential, and mRNA encapsulation (Fig. S11†) and no differences were observed that explained the results of the *in vivo* mRNA delivery. After IV injection, we were able to obtain spleen specific delivery at 20 and 30%.

Since 20% incorporation enabled the highest luminescence, we decided to focus on a series of formulations at 20% to study the remaining PLs as SORT molecules. The LNPs containing 4ME, POPE and DSPC achieved similar delivery efficiency to the liver when incorporated into the SORT formulation at 20%. Interestingly, CL-LNP exhibited spleen-specific delivery although lower in efficacy (Fig. 6C). These results indicate that choice of PLs in a four component LNP increase overall delivery efficiency. Moreover, in the context of SORT LNPs, PLs can change organ tropism from liver to spleen and further increase spleen delivery efficacy.

Conclusions

The field of mRNA therapeutics has quickly gained importance due to the worldwide impact of mRNA LNP vaccines. As the mRNA field moves forward, it is important to understand the fundamental role(s) of all lipid components that comprise LNPs. Although efforts have mainly focused on the ionizable cationic lipid, understanding the role of the other molecules within LNPs are important for safety and efficacy. Here, we demonstrated that the chemistry of the phospholipid plays an important role in endosomal escape and can enhance the delivery of mRNA both *in vitro* and *in vivo* when incorporated as part of a 4-component LNP. Furthermore, we demonstrated that negatively charged lipids drive spleen tropism *in vivo* in the context of 4- and 5-component SORT LNPs. Together these results break the paradigm of the phospholipid being considered as a "helper lipid". It has also been observed that PLs can alter the activity of LNPs designed for siRNA and DNA.[46,65,66] Studying the roles of PLs in additional LNP types and for different cargoes is an important area of ongoing and future research. Moreover, we demonstrated how alternative phospholipids in LNP formulations can enhance delivery and offer organ targeting. Enhanced *in vivo* delivery of mRNA LNPs *via* inclusion of PLs with higher endosomal escape potential is expected to lead to improved mRNA vaccines against SARS-CoV-2 and future viruses, as well as improve development of novel therapeutics against a variety of diseases.

Author contributions

Ester Álvarez-Benedicto: conceptualization, methodology, investigation, formal analysis, writing – original draft, writing – review & editing, visualization, funding acquisition. Lukas Farbiak: conceptualization, methodology, investigation, writing – review & editing, visualization. Martha Márquez Ramírez: investigation, writing – review & editing. Lindsay T. Johnson: investigation, writing – review & editing. Xu Wang: investigation. Osamah Mian: investigation, writing – review & editing. Erick D. Guerrero: investigation. Daniel J. Siegwart: conceptualization, methodology, resources, writing – review & editing, supervision, project administration, funding acquisition.

Conflicts of interest

There are no conflicts to declare.

Acknowledgements

D. J. S. acknowledges financial support from the National Institutes of Health (NIH) National Institute of Biomedical Imaging and Bioengineering (NIBIB) (R01 EB025192-01A1), the Cystic Fibrosis Foundation (CFF) (SIEGWA18XX0), the Cancer Prevention and Research Institute of Texas (CPRIT) (RP190251), the American Cancer Society (ACS) (RSG-17-012-01), and the Welch Foundation (I-1855). We acknowledge the UTSW Tissue Resource, supported in part by the National Cancer Institute (5P30CA142543), and the Moody Foundation Flow Cytometry Facility. E. A. B acknowledges financial support from the National Science Foundation Graduate Research Fellowship Program (NSF GRFP) (2018270395). D. J. S. and E. A. B. acknowledge support from the Howard Hughes Medical Institute (GT15136).

Notes and references

1 P. R. Cullis and M. J. Hope, *Mol. Ther.*, 2017, **25**, 1467–1475.
2 K. Whitehead, R. Langer and D. Anderson, *Nat. Rev. Drug Discovery*, 2009, **8**, 129–138.
3 R. Kanasty, J. R. Dorkin, A. Vegas and D. Anderson, *Nat. Mater.*, 2013, **12**, 967–977.
4 K. J. Kauffman, M. J. Webber and D. G. Anderson, *J. Controlled Release*, 2016, **240**, 227–234.
5 H. X. Wang, M. Li, C. M. Lee, S. Chakraborty, H. W. Kim, G. Bao and K. W. Leong, *Chem. Rev.*, 2017, **117**, 9874–9906.
6 K. A. Hajj and K. A. Whitehead, *Nat. Rev. Mater.*, 2017, **2**, 17056.
7 J. B. Miller and D. J. Siegwart, *Nano Res.*, 2018, **11**, 5310–5337.
8 T. Wei, Q. Cheng, L. Farbiak, D. G. Anderson, R. Langer and D. J. Siegwart, *ACS Nano*, 2020, **14**, 9243–9262.
9 M. J. Mitchell, M. M. Billingsley, R. M. Haley, M. E. Wechsler, N. A. Peppas and R. Langer, *Nat. Rev. Drug Discovery*, 2021, **20**, 101–124.
10 A. Akinc, M. A. Maier, M. Manoharan, K. Fitzgerald, M. Jayaraman, S. Barros, S. Ansell, X. Du, M. J. Hope, T. D. Madden, B. L. Mui, S. C. Semple, Y. K. Tam, M. Ciufolini, D. Witzigmann, J. A. Kulkarni, R. van der Meel and P. R. Cullis, *Nat. Nanotechnol.*, 2019, **14**, 1084–1087.
11 L. A. Jackson, E. J. Anderson, N. G. Rouphael, P. C. Roberts, M. Makhene, R. N. Coler, M. P. McCullough, J. D. Chappell, M. R. Denison, L. J. Stevens, A. J. Pruijssers, A. McDermott, B. Flach, N. A. Doria-Rose, K. S. Corbett, K. M. Morabito, S. O'Dell, S. D. Schmidt, P. A. Swanson, II, M. Padilla, J. R. Mascola, K. M. Neuzil, H. Bennett, W. Sun, E. Peters, M. Makowski, J. Albert, K. Cross, W. Buchanan, R. Pikaart-Tautges, J. E. Ledgerwood, B. S. Graham and J. H. Beigel, *N. Engl. J. Med.*, 2020, **383**, 1920–1931.
12 A. Wittrup, A. Ai, X. Liu, P. Hamar, R. Trifonova, K. Charisse, M. Manoharan, T. Kirchhausen and J. Lieberman, *Nat. Biotechnol.*, 2015, **33**, 870–876.
13 J. Gilleron, W. Querbes, A. Zeigerer, A. Borodovsky, G. Marsico, U. Schubert, K. Manygoats, S. Seifert, C. Andree, M. Stoter, H. Epstein-Barash, L. Zhang, V. Koteliansky, K. Fitzgerald, E. Fava, M. Bickle, Y. Kalaidzidis, A. Akinc, M. Maier and M. Zerial, *Nat. Biotechnol.*, 2013, **31**, 638–646.
14 I. M. Hafez, N. Maurer and P. R. Cullis, *Gene Ther.*, 2001, **8**, 1188–1196.
15 S. C. Semple, A. Akinc, J. X. Chen, A. P. Sandhu, B. L. Mui, C. K. Cho, D. W. Y. Sah, D. Stebbing, E. J. Crosley, E. Yaworski, I. M. Hafez, J. R. Dorkin, J. Qin, K. Lam, K. G. Rajeev, K. F. Wong, L. B. Jeffs, L. Nechev, M. L. Eisenhardt, M. Jayaraman, M. Kazem, M. A. Maier, M. Srinivasulu, M. J. Weinstein, Q. M. Chen, R. Alvarez, S. A. Barros, S. De, S. K. Klimuk, T. Borland, V. Kosovrasti, W. L. Cantley, Y. K. Tam, M. Manoharan, M. A. Ciufolini, M. A. Tracy, A. de Fougerolles, I. MacLachlan, P. R. Cullis, T. D. Madden and M. J. Hope, *Nat. Biotechnol.*, 2010, **28**, 172–176.
16 D. F. Zhi, S. B. Zhang, S. H. Cui, Y. A. Zhao, Y. H. Wang and D. F. Zhao, *Bioconjugate Chem.*, 2013, **24**, 487–519.
17 K. Zhou, L. H. Nguyen, J. B. Miller, Y. Yan, P. Kos, H. Xiong, L. Li, J. Hao, J. T. Minnig, H. Zhu and D. J. Siegwart, *Proc. Natl. Acad. Sci. U. S. A.*, 2016, **113**, 520–525.
18 O. Zelphati and F. C. Szoka, Jr., *Proc. Natl. Acad. Sci. U. S. A.*, 1996, **93**, 11493–11498.
19 N. Pardi, S. Tuyishime, H. Muramatsu, K. Kariko, B. L. Mui, Y. K. Tam, T. D. Madden, M. J. Hope and D. Weissman, *J. Controlled Release*, 2015, **217**, 345–351.
20 S. Ramishetti, I. Hazan-Halevy, R. Palakuri, S. Chatterjee, S. Naidu Gonna, N. Dammes, I. Freilich, L. Kolik Shmuel, D. Danino and D. Peer, *Adv. Mater.*, 2020, **32**, e1906128.
21 K. Paunovska, A. J. D. Sanchez, C. D. Sago, Z. B. Gan, M. P. Lokugamage, F. Z. Islam, S. Kalathoor, B. R. Krupczak and J. E. Dahlman, *Adv. Mater.*, 2019, **31**, 1807748.
22 S. Patel, N. Ashwanikumar, E. Robinson, Y. Xia, C. Mihai, J. P. Griffith, S. Hou, A. A. Esposito, T. Ketova, K. Welsher, J. L. Joyal, O. Almarsson and G. Sahay, *Nat. Commun.*, 2020, **11**, 983.
23 Y. J. Bao, Y. Jin, P. Chivukula, J. Zhang, Y. Liu, J. Liu, J. P. Clamme, R. I. Mahato, D. Ng, W. B. Ying, Y. T. Wang and L. Yu, *Pharm. Res.*, 2013, **30**, 342–351.
24 Q. G. Xu, L. M. Ensign, N. J. Boylan, A. Schon, X. Q. Gong, J. C. Yang, N. W. Lamb, S. T. Cai, T. Yu, E. Freire and J. Hanes, *ACS Nano*, 2015, **9**, 9217–9227.
25 X. W. Cheng and R. J. Lee, *Adv. Drug Delivery Rev.*, 2016, **99**, 129–137.
26 B. L. Mui, Y. K. Tam, M. Jayaraman, S. M. Ansell, X. Y. Du, Y. Y. C. Tam, P. J. C. Lin, S. Chen, J. K. Narayanannair, K. G. Rajeev, M. Manoharan, A. Akinc, M. A. Maier, P. Cullis, T. D. Madden and M. J. Hope, *Mol. Ther.–Nucleic Acids*, 2013, **2**, e139.
27 S. C. Wilson, J. L. Baryza, A. J. Reynolds, K. Bowman, M. E. Keegan, S. M. Standley, N. P. Gardner, P. Parmar, V. O. Agir, S. Yadav, A. Zunic, C. Vargeese, C. C. Lee and S. Rajan, *Mol. Pharm.*, 2015, **12**, 386–392.
28 K. A. Whitehead, J. Matthews, P. H. Chang, F. Niroui, J. R. Dorkin, M. Severgnini and D. G. Anderson, *ACS Nano*, 2012, **6**, 6922–6929.
29 A. D. Bangham, M. M. Standish and J. C. Watkins, *J. Mol. Biochem.*, 1965, **13**, 238–IN227.
30 P. R. Cullis, M. J. Hope and C. P. S. Tilcock, *Chem. Phys. Lipids*, 1986, **40**, 127–144.
31 R. Yang, X. Zhang, F. Li, L. Ding, B. Li, H. Sun and Y. Gan, *Colloids Surf., A*, 2013, **436**, 434–442.
32 R. Kolašinac, C. Kleusch, T. Braun, R. Merkel and A. Csiszár, *Int. J. Mol. Sci.*, 2018, **19**, 346.
33 V. K. Sharma, K. K. Sarwa and B. Mazumder, *J. Liposome Res.*, 2014, **24**, 83–89.
34 C. Rupp, H. Steckel and B. W. Müller, *Int. J. Pharm.*, 2010, **395**, 272–280.

35 M. Anderson and A. Omri, *Drug Delivery*, 2004, **11**, 33–39.
36 G. Gregoriadis, P. D. Leathwood and B. E. Ryman, *FEBS Lett.*, 1971, **14**, 95–99.
37 T. M. Allen and P. R. Cullis, *Adv. Drug Delivery Rev.*, 2013, **65**, 36–48.
38 M. H. Gaber, K. Hong, S. K. Huang and D. Papahadjopoulos, *Pharm. Res.*, 1995, **12**, 1407–1416.
39 F. Passero, D. Grapsa, K. Syrigos and W. Saif, *Expert Rev. Anticancer Ther.*, 2016, **16**, 697–703.
40 E. A. Forssen and M. E. Ross, *J. Liposome Res.*, 1994, **4**, 481–512.
41 R. Zhang, R. El-Mayta, T. J. Murdoch, C. C. Warzecha, M. M. Billingsley, S. J. Shepherd, N. Gong, L. Wang, J. M. Wilson, D. Lee and M. J. Mitchell, *Biomater. Sci.*, 2021, **9**, 1449–1463.
42 A. K. K. Leung, I. M. Hafez, S. Baoukina, N. M. Belliveau, I. V. Zhigaltsev, E. Afshinmanesh, D. P. Tieleman, C. L. Hansen, M. J. Hope and P. R. Cullis, *J. Phys. Chem. C*, 2012, **116**, 22104–22104.
43 J. B. Miller, S. Zhang, P. Kos, H. Xiong, K. Zhou, S. S. Perelman, H. Zhu and D. J. Siegwart, *Angew. Chem., Int. Ed.*, 2017, **56**, 1059–1063.
44 K. J. Kauffman, J. R. Dorkin, J. H. Yang, M. W. Heartlein, F. DeRosa, F. F. Mir, O. S. Fenton and D. G. Anderson, *Nano Lett.*, 2015, **15**, 7300–7306.
45 Y. Dong, J. R. Dorkin, W. Wang, P. H. Chang, M. J. Webber, B. C. Tang, J. Yang, I. Abutbul-Ionita, D. Danino, F. DeRosa, M. Heartlein, R. Langer and D. G. Anderson, *Nano Lett.*, 2016, **16**, 842–848.
46 J. A. Kulkarni, D. Witzigmann, J. Leung, Y. Y. C. Tam and P. R. Cullis, *Nanoscale*, 2019, **11**, 21733–21739.
47 J. Li, X. Wang, T. Zhang, C. Wang, Z. Huang, X. Luo and Y. Deng, *Asian J. Pharm. Sci.*, 2015, **10**, 81–98.
48 G. van Meer, D. R. Voelker and G. W. Feigenson, *Nat. Rev. Mol. Cell Biol.*, 2008, **9**, 112–124.
49 S. Simões, V. Slepushkin, N. Düzgünes and M. C. Pedroso De Lima, *Biochim. Biophys. Acta, Biomembr.*, 2001, **1515**, 23–37.
50 H. Ellens, J. Bentz and F. C. Szoka, *Biochemistry*, 1984, **23**, 1532–1538.
51 B. Li, X. Luo, B. Deng, J. Wang, D. W. McComb, Y. Shi, K. M. Gaensler, X. Tan, A. L. Dunn, B. A. Kerlin and Y. Dong, *Nano Lett.*, 2015, **15**, 8099–8107.
52 Q. Cheng, T. Wei, Y. Jia, L. Farbiak, K. Zhou, S. Zhang, Y. Wei, H. Zhu and D. J. Siegwart, *Adv. Mater.*, 2018, **30**, e1805308.
53 Z. Du, M. M. Munye, A. D. Tagalakis, M. D. I. Manunta and S. L. Hart, *Sci. Rep.*, 2014, **4**, 7107.
54 K. K. L. Phua, H. F. Staats, K. W. Leong and S. K. Nair, *Sci. Rep.*, 2015, **4**, 5128.
55 N. Veiga, M. Goldsmith, Y. Granot, D. Rosenblum, N. Dammes, R. Kedmi, S. Ramishetti and D. Peer, *Nat. Commun.*, 2018, **9**, 4493.
56 Y. Yan, L. Liu, H. Xiong, J. B. Miller, K. Zhou, P. Kos, K. E. Huffman, S. Elkassih, J. W. Norman, R. Carstens, J. Kim, J. D. Minna and D. J. Siegwart, *Proc. Natl. Acad. Sci. U. S. A.*, 2016, **113**, E5702–E5710.
57 S. M. Lee, Q. Cheng, X. Yu, S. Liu, L. T. Johnson and D. J. Siegwart, *Angew. Chem., Int. Ed.*, 2021, **60**, 5848–5853.
58 S. Liu, Q. Cheng, T. Wei, X. Yu, L. T. Johnson, L. Farbiak and D. J. Siegwart, *Nat. Mater.*, 2021, **20**, 701–710.
59 Q. Cheng, T. Wei, L. Farbiak, L. T. Johnson, S. A. Dilliard and D. J. Siegwart, *Nat. Nanotechnol.*, 2020, **15**, 313–320.
60 T. Wei, Q. Cheng, Y.-L. Min, E. N. Olson and D. J. Siegwart, *Nat. Commun.*, 2020, **11**, 3232.
61 H. Xiong, S. Liu, T. Wei, Q. Cheng and D. J. Siegwart, *J. Controlled Release*, 2020, **325**, 198–205.
62 L. Farbiak, Q. Cheng, T. Wei, E. Alvarez-Benedicto, L. T. Johnson, S. Lee and D. J. Siegwart, *Adv. Mater.*, 2021, **33**, e2006619.
63 A. P. French, S. Mills, R. Swarup, M. J. Bennett and T. P. Pridmore, *Nat. Protoc.*, 2008, **3**, 619–628.
64 S.-T. Yang, E. Zaitseva, L. V. Chernomordik and K. Melikov, *Biophysi. J.*, 2010, **99**, 2525–2533.
65 Y. Sato, H. Hatakeyama, Y. Sakurai, M. Hyodo, H. Akita and H. Harashima, *J. Controlled Release*, 2012, **163**, 267–276.
66 I. Ermilova and J. Swenson, *Phys. Chem. Chem. Phys.*, 2020, **22**, 28256–28268.